Numerical Detector Theory for the Longitudinal Momentum Distribution of the Electron in Strong Field Ionization

Justin Tian, Xu Wang, and J. H. Eberly

Numerical Detector Theory for the Longitudinal Momentum Distribution of the Electron in Strong Field Ionization

Justin Tian[1],[*] Xu Wang[2],[†] and J. H. Eberly[1]

[1] Department of Physics & Astronomy, University of Rochester, Rochester, New York, 14627, USA and
[2] Graduate School, China Academy of Engineering Physics, Beijing 100193, China

(Dated: April 21, 2017)

The lack of analytical solutions for the exit momentum in laser-driven tunneling theory is a well recognized problem in strong field physics. Theoretical studies of electron momentum distributions in the neighborhood the tunneling exit depend heavily on ad hoc assumptions. In this report, we apply a new numerical method to study exiting longitudinal electron momentum distribution under intense short-pulse laser excitation. We present the first realizations of the dynamic behavior of an electron near the so-called tunneling exit region without adopting a tunneling approximation.

PACS numbers: 32.80.Fb, 32.80.Rm

Strong-field AMO physics is an exceptional domain in science. For several decades it has been yielding an array of unexpected and sometimes strongly counter-intuitive experimental findings. It has done this just by combining long-familiar elements (atoms and photons) at high laser field strengths on a very short time scale. It is one of the few domains in physics where non-perturbative theory can confront feasible experiments that enter new parameter spaces, in this case the realm of attoscience. Here we take two steps that resolve an existing strong-field conflict and in doing so provide long-needed ab initio results which show time dependent oscillations in the momentum of an electron in the vicinity of what is called the tunneling exit.

Ionization is an essential element of strong-field AMO physics because it is the first step leading to some of the most intriguing phenomena including, for instance, high harmonic generation (HHG) [1], non-sequential double ionization (NSDI) [2, 3] and the arena of attosecond science generally [4]. Semi-classical models are the dominant theoretical approach in studying strong field ionization. In such a model, an electron first non-perturbatively tunnels through a tilted Coulomb potential barrier, and then flies away along a classical trajectory [5, 6].

A typical semi-classical simulation model depends on the widely used 'adiabatic' tunneling condition [7, 8], which adopts the approximation that the ionizing laser frequency is much slower than the bound electron's Bohr frequency. However, in recent years, the adiabatic tunneling theory has been challenged [9–13]. These advanced studies raise the question: if the tunneling process is non-adiabatic and significantly time-dependent, how do we describe an electron's momentum distribution near the tunneling exit point, especially its momentum component longitudinal to the laser field's major polarization axis?

We emphasize the longitudinal momentum here since the distributed wave function of an electron that is nominally under the potential barrier can be strongly affected by the laser in the direction of the field. Some theoretical results [14, 15] provide approximate formulas for the asymptotic longitudinal momentum, but accurate analytical expressions are not known for the 'exit' longitudinal momentum or its standard deviation at the tunneling exit point. The difficulty to be expected in overcoming this lack has been recently noticed and emphasized by the strong-field physics community [16–18] and the earliest analysis of this issue remains prominently relevant:

"··· Uncertainty in the moment of tunneling, which is responsible for the uncertainty in the initial velocity, also means that it is virtually impossible to separate the initial velocity distribution from the distortions caused by the electric field during this temporal uncertainty." [19].

When physicists adopt an adiabatic tunneling model in studying longitudinal momentum, they may easily find controversial results. Pfeiffer *et al.* and Sun *et al.* have used similar experimental techniques to reveal the momentum distributions at the tunneling exit for helium and krypton atoms [16, 18]. A coordinated backward processing method has been employed by both groups to find values and standard deviations of the exit's longitudinal momentum.

In the backward processing method, in the first step, an electron is assumed to tunnel through the potential barrier and to appear outside the barrier with some probability. The timing and position of the tunneling electron and its ionization probability are decided by the adiabatic tunneling model. Then, by randomly choosing from a presumed distribution, one assigns a momentum to the tunneled electron. The longitudinal component of this artificial momentum distribution is a gaussian distribution centered at zero and has a presumed standard deviation [16]. In the second step, one uses the tunneling exit position and the tunneling probability given by the ionization model and the model momentum as the initial

conditions of a classical trajectory. By comparing the numerical far-field (asymptotic) momentum distributions (especially the longitudinal part) against the experimental data at different ellipticities, one finds the exit longitudinal momentum standard deviation values that give the least absolute error between the numerical results and the experimental data. Both groups [16, 18] conclude that this backward processing method can define the exit longitudinal momentum distributions for different ellipticities at the tunneling exit point. Surprisingly, the same approach leads to contradictory conclusions.

By applying backward processing and making a strict quantitative comparison between data and simulating results, Pfeiffer *et al.* have found that the tunneling electron emerges with a non-zero standard deviation ranging from 0.5 (ε=0.55) to 1.3 (ε=0.15) atomic units (a.u.) in its exit longitudinal momentum [16]. Hofmann *et al.* reconfirmed that a non-zero exit longitudinal momentum spread is crucial to reach quantitative agreement between the numerical and experimental data [17].

However, using experimental observations of krypton ionization, Sun *et al.* [18] and Li *et al.* [20] reach an opposite conclusion. They compare the longitudinal momentum data of krypton to backward processing simulations and demonstrate that near-zero choices of the exit longitudinal momentum standard deviation between 0.0 and 0.2 a.u. are more credible. Sun *et al.* conclude that a zero exit longitudinal momentum width is still a valid exit momentum distribution to use in a semi-classical model.

These two different conclusions show that the exit longitudinal momentum distributions given by a backward processing method may heavily depend on the initial-condition assumptions.

In any discussion of ionization, it is important to remain aware that experiments have no direct access to electron behavior at the 'moment' or 'location' of a 'tunnel exit' or 'release' from the ion, if such non-quantum language even makes sense. These artificial 'initial' conditions of classical trajectories are used in almost all semi-classical models due to the absence of a full analytical expression of the tunneling ionization. In recent advanced experiments using strong ultra-fast laser pulses, the tunneling ionization model has begun to lose its predictive power. One can always retrieve a best fitting result by manipulating the initial conditions. In such cases, a semi-classical model regresses to a mere mathematical tool.

By contrast, exploration of the confusion/conflict about important features of the exit momenta is very direct when using the SENE (Schrödinger equation - Newton equation) method, which has been introduced and extended in [21, 22]. It provides, we believe, the first results that are not under the control of a tunneling assumption. Both longitudinal and transverse standard deviations, as well as correlations can be calculated. As far as a 'tunnel exit' is concerned, the distribution of times of arrival to almost any exit point is also available.

In this report, we show that the SENE method can not only resolve the conflict between experiments, but also can help in retrieving the dynamical behavior of an electron near the imprecisely known tunneling zone. We follow the laboratory conditions used for helium and krypton atoms [16, 18] and first numerically solve a two-dimensional TDSE in the polarization plane (x-y plane) for the quantum wave function in a soft-core Coulomb potential $V = -1/\sqrt{a^2 + r^2}$ [25, 26], where the bound-electron's wave function $\Psi(\vec{r}, t)$ at $t = 0$ is numerically found by imaginary time integration. We use $a = 0.28$ (0.5) a.u. to have a ground state energy of -0.9 (-0.51) a.u. to match the ionization potential of helium (krypton). A laser pulse starts to interact with the wave function at $t = 0$. The laser field $\vec{E}(t)$ in a.u. is given by

$$\vec{E}(t) = \sqrt{\frac{I}{1+\varepsilon^2}} f(t)[\sin(\omega t + \zeta)\hat{e}_x + \varepsilon \cos(\omega t + \zeta)\hat{e}_y] \quad (1)$$

For helium calculations, the laser field has a wavelength of 788 nm and a FWHM of 33fs. The peak laser intensity is I=0.8 PW/cm^2, $f(t)$ is a sine-squared shape envelope function which has maximum value 1 and ζ is the carrier-envelope phase (CEP) [27]. For krypton, the wavelength is still 788nm, but the peak intensity drops to 0.12PW/cm^2 and the FWHM drops to 25fs. We apply the SENE with different ε values ranging from 0.2 to 0.93. To mimic a random CEP, we use five CEPs evenly distributed between $(0, 2\pi)$ for each ε value. The size of our discrete numerical time step is 0.02 a.u.

To confirm that the SENE results can lead to a quantitative agreement with experimental data, we have also compared our numerical far-field longitudinal momentum standard deviations σ_x^{ff} with experiment [16]. We follow the definition of the longitudinal momentum standard deviations in [14, 16]. The asymptotic longitudinal momentum is defined as the momentum component along the major polarization direction (x-axis). In Fig. 1, we include experimental data from [16], and a theory function curve from [14]. The formula for the theory line is $\sigma_x^{ff} = \sqrt{3\omega/2\gamma^3(1 - \varepsilon^2)}$.

Comparing with a tunneling semi-classical model, the SENE competitive advantage is obvious. One does not need to rely on the unprovable presumption that an electron is ionized through tunneling despite being exposed to unknown dynamical effects, and finally appears outside the barrier with a specific momentum and a zero tunneling time. Instead, all information is obtained by integrating the TDSE and is extracted by numerical detectors (ND) described previously [21, 22]. By splitting the computing space into an inner part and an outer part, the SENE method shares some common features with other advanced numerical methods (e.g., ARM by Barth, et al. [23], t-SURFF by Scrinzi [24]).

In recent researches, the SENE method has been proved a useful model in studying non-adiabatic tunneling process with a non-zero tunneling time delay [28, 29].
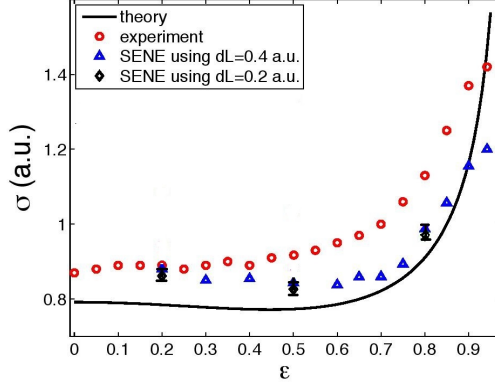
FIG. 1: The final momentum spread in the x direction. In this graph, we show σ_x^{ff} values of a theory line (black solid line) [14], experiment data points (red circles) [16], and the SENE result using grid map step size $dL =0.4$ a.u. (blue triangles). At $\varepsilon =0.2$, 0.5 and 0.8, we also show the SENE results using $dL =0.2$ as a 'theoretical error bar'. The results of $dL = 0.4$ and 0.2 converge at all three ellipticities.

However, the electron's dynamic motion under the barrier is still an unsolved question. In this paper, we use numerical detectors [21] to study the momentum distributions of the wave-function near the 'tunneling' region and directly observe the electron's behavior in a classical forbidden zone without using a tunneling hypothesis or approximations.

To investigate the momentum distributions near the tunneling zone, we set the ND ring's radius close to the postulated laser cycle averaged tunneling 'radius'. In a linearly polarized field, this is approximately $I_p/|E_t|$, where I_p is the ionization potential of the electron and $|E_t|$ is the field strength at time t. For helium, with the laser parameters used in our calculations, the tunneling radius is about 6 a.u. at the peak intensity of the laser pulse. The same approximation gives a tunneling radius for krypton which is about 8 a.u. Considering the time dependent oscillation of the laser field, and that the field strength decreases with larger ellipticity values, we set the ND circle at 10 a.u for both helium and krypton to collect the momentum information near the tunneling region. In Fig. 2, we show the scheme of the SENE method.

In Fig. 3 we show cumulative exit momentum distributions for helium and krypton through the laser pulse. The exit momentum distributions are collected by the NDs. In the distributions of helium atoms, along the p_x axis, all distributions divide into two parts and form a two-peak structure. To capture the dynamic motion of an electron near the tunneling exit, we use the data values recorded by NDs in a time window with size T/8, where T is the laser cycle period. There are approximately 250 time steps in each time window. Since the CEP value is specified for each ionized electron, we will
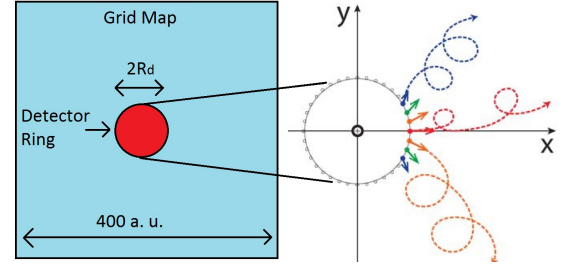

FIG. 2: The circle of numerical detectors [21, 22] with radius R_d is shown, as well as outgoing classical particle trajectories that were initiated with the momentum values determined by the detectors. The trajectories continue to be fully affected by both laser action and ionic Coulomb attraction as the particles propagate outward to actual detection.
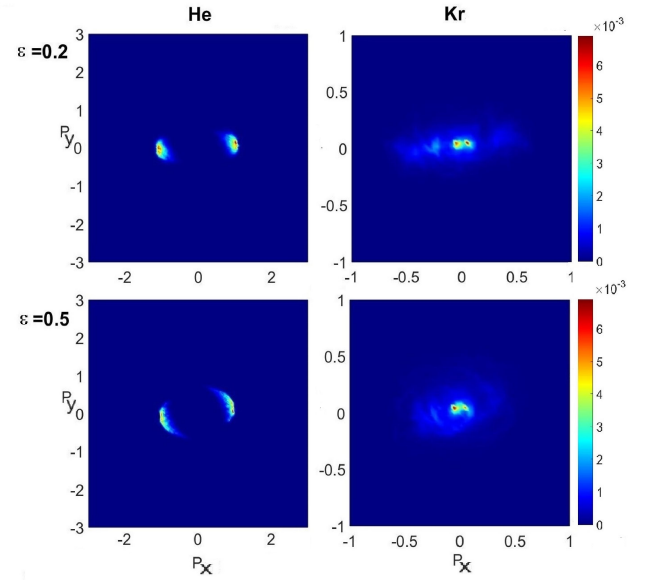

FIG. 3: Rows from top to bottom: $\varepsilon =0.2$, 0.5. Columns from left to right: cumulative initial momentum distributions in the polarization (x-y) plane at NDs through whole laser pulse of (1) helium, (2) krypton. The peak laser intensities used are for helium 0.8 PW/cm^2, and for krypton 0.12 PW/cm^2.

use only zero CEP to demonstrate an electron's motion. For other CEPs, the time oscillation curves will simply shift.

We plot the averaged exit momentum-distribution parameters in Fig. 4. In the plot, both time resolved parameters of helium and krypton show a time dependent oscillation. Although the oscillating amplitude of krypton is much smaller than that of helium, the time-dependent average momenta, $\bar{p}_x$ and $\bar{p}_y$, of krypton still have non-zero values and oscillate around zero. The time-dependent oscillation of the average longitudinal momentum confirms that the electron's momentum near the tunneling region is time dependent and should be described in a dynamic way. Clearly, an electron's motion
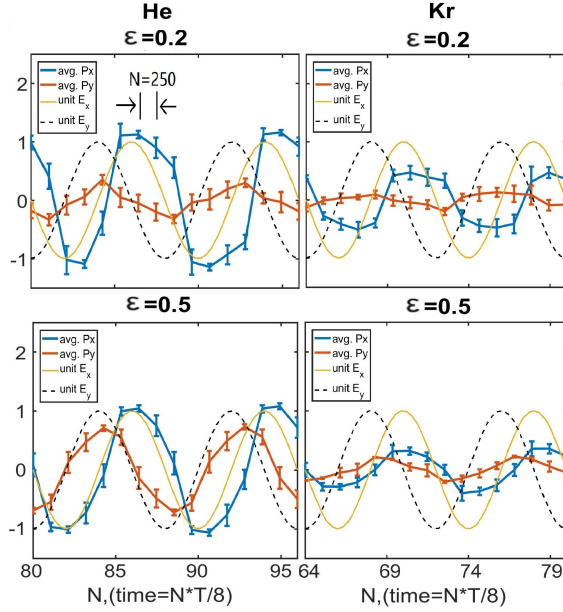
FIG. 4: Time resolved values of $\bar{p}_{xt}$, $\bar{p}_{yt}$, T is one laser period. The discrete step size is $T/8$. The width of the momentum distribution in each time window is plotted as vertical error bars. Columns from left to right: (1) helium, (2) krypton. All single plots show the time dependent parameters' changes over the center two and half cycles of the laser pulse. We also plot unit field oscillation in both x and y directions.

near the tunneling region is non-adiabatic and strongly coupled with the laser field. In Fig. 4, we also plot the unit field strengths.

However, these time oscillations of a single electron cannot be observed in a lab now (nor in the foreseeable future). For experimental observations, it's meaningful to describe the electron's initial momentum in a cumulative ensemble by including data from all times and all CEPs.

So, we plot the cumulative $\sigma(p_x)$ and $\sigma(p_y)$ in Fig. 5. First, we notice that the standard deviations of p_y of helium and krypton at $\varepsilon < 0.5$ are close to the values predicted by the tunneling theory. The tunneling theory [7, 8] predicts that the exit momentum component perpendicular to the polarization direction has a gaussian distribution, which is centered at zero and has a standard deviation equal to

$$\sigma_{tunnel}(p_y) = \sqrt{\frac{\omega}{2\gamma}}, \quad \gamma = \frac{\omega\sqrt{2I_p(1+\varepsilon^2)}}{E_0} \quad (2)$$

Here, γ is the Keldysh parameter [30], and ω, I and ε are the laser field's frequency, peak intensity and ellipticity. With a linearly polarized field, Eq. 2 gives standard deviation values of 0.24 a.u. for helium and 0.17 a.u. for krypton. In Fig. 5, at $\varepsilon < 0.5$, $\sigma(p_y)$ values of both helium and krypton are close to the predicted values.

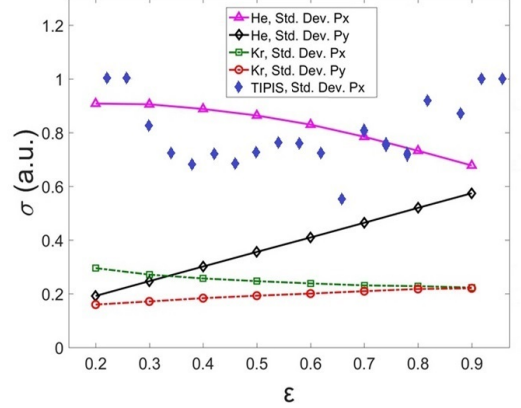When the ellipticity increases, two pairs of numerical curves of helium and krypton behave in a similar way.

FIG. 5: This figure shows how the cumulative $\sigma(p_x)$ and $\sigma(p_y)$ change vs. ellipticities for helium and krypton atoms. In a near-circularly polarized laser beam, two standard deviations converge. We also compare our data of standard deviations in longitudinal momentum of helium atoms to the prediction made by the TIPIS model [16].

Standard deviations in p_x and p_y directions, $\sigma(p_x)$ and $\sigma(p_y)$, will converge toward a single value when the ellipticity goes to 1. That is, in a circularly polarized laser field, the exit momentum distribution is uniformly distributed along a circle. The cumulative momenta standard deviations mimic the behavior of E_{0x} and E_{0y} when the ellipticity changes, which are proportional to $\sqrt{1/(1+\varepsilon^2)}$ and $\sqrt{\varepsilon^2/(1+\varepsilon^2)}$. That explains why $\sigma(p_y)$ is more sensitive to the ellipticity change.

The longitudinal momentum standard deviations of krypton are much smaller than for helium at all ellipticity values. Our longitudinal momentum standard deviations of krypton (green dash line) range from 0.3 to 0.22 a.u. This standard deviation range is in the range of the prediction made by Sun et al. [18].

Surprisingly, our momentum standard deviations near the tunneling region quantitatively agree with both groups' results. There is no controversy in our simulations. Near-one and near-zero standard deviations coexist in our results.

In the view of the SENE method, the decrease of the exit longitudinal momentum standard deviation is a predictable result. An outgoing wave packet will be accelerated and stretched in the direction of the laser field. When the laser peak intensity drops from 0.8 PW/cm^2 to 0.12 PW/cm^2, a smaller average $|p_x|$ value and a smaller $\sigma(p_x)$ are predictable results with the SENE method. The actual conflicts come from overlooking the coupling between the laser field and the ionized electron's momentum. In the backward processing, both groups assume that an electron is ionized through adiabatic tunneling. In the cumulative momentum distribution plots, due to

a higher laser intensity, the separation between the two peaks is larger for helium atoms. To cover the larger separation, the adiabatic hypothesis needs larger standard deviations. In Fig. 5, the TIPIS model [16] predicts standard deviations that are close to our data of helium atoms. So, using a backward process, one can partially match the physical truth of the longitudinal momenta. However, such an adiabatic hypothesis misses the crucial coupling between the laser and the ionized electron which is easily handled by the SENE method.

In conclusion, in past research, the adiabatic tunneling theory has been a powerful theoretical tool to interpret experimental data. In this report, we note that using adiabatic assumptions in studying the longitudinal momentum distributions of photo-ionized electrons can lead to controversial conclusions. We show how the SENE method can resolve controversies caused by a backward processing method. Using the SENE method, we retrieve the first quantitative evidence of dynamic motion of an electron near the tunneling region. Since the SENE method can easily retrieve quantum wavefunction information of an electron, it will be a valuable tool for ab initio studies including both laser and ionic forces. In the so-called tunneling zone, fascinating issues such as the electron's multidimensional motion and its dynamic delay time must be the topics of future work. This research is supported by the DOE grant DE-FG02-05ER15713.

---

[1] A. L'Huillier, L. Lompre, G. Mainfray, and C. Manus, Atoms in Intense Laser Fields, edited by M. Gavrila (Academic Press, New York, 1992).
[2] D. N. Fittinghoff, P. R. Bolton, B. Chang, and K. C. Kulander, Phys. Rev. Lett. **69**, 2642 (1992).
[3] W. Becker, X. J. Liu, P. J. Ho, and J. H. Eberly, Rev. Mod. Phys. **84**, 1011 (2012).
[4] F. Krausz and M. Ivanov, Rev. Mod. Phys. **81**, 163 (2009).
[5] C. Liu and K. Z. Hatsagortsyan, Phys. Rev. Lett. **105**, 113003 (2010).
[6] D. Dimitrovski and L. B. Madsen, Phys. Rev. A **91**, 033409 (2015).
[7] M. V. Ammosov, N. B. Delone, and V. P. Krainov, Sov. Phys. JETP **64**, 1191 (1986).
[8] N. B. Delone and V. P. Krainov, J. Opt. Soc. Am. B **8**, 1207 (1991).
[9] D. Shafir, H. Soifer, B. D. Bruner, M. Dagan, Y. Mairesse, S. Patchkovskii, M.Yu. Ivanov, O. Smirnova, and N. Dudovich, Nature (London) **485**, 343 (2012).
[10] R. Boge, C. Cirelli, A. S. Landsman, S. Heuser, A. Ludwig, J. Maurer, M. Weger, L. Gallmann, and U. Keller, Phys. Rev. Lett. **111**, 103003 (2013).
[11] I. A. Ivanov and A. S. Kheifets, Phys. Rev. A **89** 021402 (2014).
[12] M. Klaiber, J. Z. Hatsagortsyan, and C. H. Keitel, Phys. Rev. Lett. **114**, 083001 (2015).
[13] M. Li. J-W Geng, M. Han, M-M Liu, L-Y Peng, Q-H Gong, and Y-Q Liu, Phys. Rev. A **93**, 013402 (2016).
[14] V. D. Mur, S. V. Popruzhenko, and V. S. Popov, Sov. Phys. JETP **92**, 777 (2001).
[15] A. M. Perelomov, V. S. Popov, and M. V. Terent'ev, Sov. Phys. JETP **24**, 207 (1967).
[16] For example, "... we study the longitudinal momentum spread of the electronic wave packet at the tunnel exit point, a quantity that has raised substantial interest and controversy." A. N. Pfeiffer, C. Cirelli, A. S. Landsman, M. Smolarski, D. Dimitrovski, L. B. Madsen, and U. Keller, Phys. Rev. Lett. **109**, 083002 (2012).
[17] For example, "... there is no clear way of calculating the longitudinal momentum spread at the exit point from tunneling models." C. Hofmann, A. S. Landsman, C. Cirelli, A. N. Pfeiffer, and U. Keller, J. Phys. B **46**, 125601 (2013).
[18] For example, "Much effort has been concentrated on exploring the initial longitudinal momentum spread, but it is still controversial." X. F. Sun, M. Li, J. Z. Yu, Y. K. Deng, Q. H. Gong, and Y. Q. Liu, Phys. Rev. A **89**, 045402 (2014).
[19] See earliest examination, in M. Y. Ivanov, M. Spanner, and O. Smirnova, J. Mod. Opt. **52**, 165 (2005).
[20] M. Li, Y. Q. Liu, H. Liu, Q. C. Ning, L. B. Fu, J. Liu, Y. K. Deng, C. Y. Wu, L. Y. Peng, and Q. H. Gong, Phys. Rev. Lett. **111**, 023006 (2013).
[21] Our numerical detectors were inspired by B. Feuerstein and U. Thumm, in J. Phys. B **36**, 707 (2003).
[22] X. Wang, J. Tian, and J. H. Eberly, Phys. Rev. Lett. **110**, 243001 (2013).
[23] I. Barth and O. Smirnova, Phys. Rev. A **84**, 063415 (2011).
[24] A. Scrinzi, New J. Phys. **14**, 085008 (2012.)
[25] J. Javanainen, J. H. Eberly, and Q. Su, Phys. Rev. A **38**, 3430 (1988).
[26] Q. Su and J.H. Eberly, Phys. Rev. A **44**, 5997 (1991).
[27] H. R. Telle, G. Steinmeyer, A. E. Dunlop, J. Stenger, D. H. Sutter, and U. Keller, Appl. Phys. B **69**, 327 (1999).
[28] N. Teeny, E. Yakaboylu, H. Bauke, and C. H. Keitel, Phys. Rev. Lett. **116**, 063003 (2016).
[29] H-C. Ni, U. Saalmann, and J-M Rost, Phys. Rev. Lett. **117**, 023002 (2016)..
[30] L. V. Keldysh, Zh. Eksp. Teor. Fiz. **47**, 1945 (1964) [Sov. Phys. J. **20**, 1307 (1965)].